

NUMERICAL INVESTIGATION OF A HAWKMOTH WING UNDERGOING PURE PLUNGE MOTION IN HOVER

Mürvet Bektaş¹
TOBB University of Economics
and Technology
Ankara, Turkey

Mehmet Ali Güler²
American University of the
Middle East, Kuwait;
TOBB ETU, Ankara, Turkey

Dilek Funda Kurtuluş³
Middle East Technical
University
Ankara, Turkey

ABSTRACT

*The aerodynamic phenomena of the flapping motion in hover mode is widely considered in micro air vehicle (MAV) applications. In this study, the aerodynamics of a three-dimensional rigid wing mimicked from the hawkmoth *Manduca sexta* is numerically investigated under pure plunge motion. The sinusoidal motion is provided with a user-defined function (UDF) to flap the wing, and the computational fluid dynamics (CFD) is used for the numerical analysis. This paper presents the effects of various parameters such as wingbeat frequency (f), stroke plane angle (β) and stroke amplitude (Φ) on the wing aerodynamics during hovering flight.*

INTRODUCTION

In recent years, the aerodynamic phenomena is widely studied on the low-Reynolds-number regimes to build micro air vehicles (MAVs) with the small sizes (<15 cm of wingspan) and low masses (<100 gr) by inspiring from the flying animals [Kurtulus, 2018]. There are three kinds of MAVs namely fixed wing, rotary wing and flapping wing. In comparison with the two other wing types, the flapping wings have better aerodynamic and propulsive efficiencies, and specifically they are more efficient in low velocities [Shyy et al., 2008]. Flapping wing micro air vehicles (FWMAVs) can be used for observation, search and rescue works by use of their superior flight performance, high maneuverability, being light and small in size and working quiet [Kurtulus, 2011a; Kurtulus, 2017]. In order to design and build FWMAVs by providing the force balance during flight, the wing morphology and wing kinematics of the birds/insects should be considered since the generated forces are affected by both wing geometry and wing motion [Combes et al., 2003; Kurtulus et al., 2006a; Kurtulus et al., 2006b].

In view of future FWMAV applications, the low-Reynolds-number aerodynamics in hovering flight performed by the insects are widely considered [Kurtulus et al., 2004; Kurtulus et al., 2008]. Hovering is a certain mode of flight where the body is fixed in space without a free stream velocity [Ames, 2001]. Because of not existing any free stream velocity, the fluid motion is only based on the wing motion such as purely pitching, purely plunging and combined pitching-plunging [Kurtulus et al., 2005; Kurtulus, 2011b].

¹ M.Sc. Student in Mechanical Engineering Department of TOBB ETU, Email: murvetbektas@etu.edu.tr

² Prof. in Mechanical Engineering Department of AUM and of TOBB ETU, Email: mehmet.guler@aum.edu.kw

³ Prof. in Aerospace Engineering Department of METU, Email: kurtulus@metu.edu.tr

There exist four types of hover mode namely normal hovering, hovering using a clap-fling mechanism, hovering along an inclined stroke plane and hovering along a vertical stroke plane [Maxworthy, 1981]. For an insect hovering along a specific stroke plane, the aerodynamic forces generated during the downstroke and upstroke depend on the various flight parameters such as wingbeat frequency, stroke plane angle, feathering angle and stroke amplitude. Stroke plane angle (β) is the angle between the wing stroke plane and the horizontal axis. The angle between the wing chord and the wing stroke plane is also defined as the feathering angle (α). The tobacco hawkmoth *Manduca sexta* is one of the most commonly used insect species in bio-inspired FWMAV designs because of its flying and hovering skills. In literature, many researchers studied on the hovering male (M) and female (F) hawkmoth *Manduca sexta* species which are categorized as M1, F1 and F2. Table 1 presents the flight conditions including wingbeat frequency (f), stroke plane angle (β) and stroke amplitude (Φ) for different *Manduca sexta* species to hover.

Table 1: Kinematic parameters for the hawkmoth *Manduca sexta* in hover

Species	f [s^{-1}]	β [$^{\circ}$]	Φ [$^{\circ}$]	References
M1 - A		11.0	114.5	[Willmott et al., 1997a]
M1 - B		15.5	115.1	[Willmott et al., 1997a]
M1 - C		18.5	113.5	[Willmott et al., 1997a]
M1 - Mean	26.10	15.0	114.4	[Willmott et al., 1997a]
F1 - A		17.8	121.9	[Willmott et al., 1997a]
F1 - B		17.9	123.6	[Willmott et al., 1997a]
F1 - C		13.2	118.8	[Willmott et al., 1997a]
F1 - Mean	26.30	16.3	121.4	[Willmott et al., 1997a]
F2 - A		21.8	106.5	[Willmott et al., 1997a]
F2 - B		21.1	115.7	[Willmott et al., 1997a]
F2 - C		27.2	117.4	[Willmott et al., 1997a]
F2 - Mean	25.40	23.4	113.2	[Willmott et al., 1997a]
Derived M1	26.10	23.6	114.6	[Liu et al., 1998]
Derived M1	26.10	15.0	114.6	[Nakata et al., 2012]
Derived M1	29.46	15.0	110.8	[Kim et al., 2014]

The flight characteristics belonging to the real *Manduca sexta* species [Willmott et al., 1997a] or to the artificial wing models generated by inspiring from the real parameters [Liu et al., 1998; Nakata et al., 2012; Kim et al., 2014] are shown in Table 1. The stroke plane angles for all *Manduca sexta* species are generally in the interval of 10° to 30° [Willmott et al., 1997a]. The *Manduca sexta* wings have three rotational degrees-of-freedom as the stroke positional (instantaneous stroke) angle ($\phi(t)$), feathering angle ($\alpha(t)$) and deviation angle ($\theta(t)$). This paper investigates the *Manduca sexta* wing model with the one rotational degree-of-freedom including only the stroke positional angle ($\phi(t)$) by assuming that the other angles are fixed. The simplified wing kinematics performs a pure plunge motion along the inclined and vertical stroke planes taking reference the parameters given in Table 1. This study aims to compare the aerodynamic forces generated on the wing for different wingbeat frequencies, stroke plane angles and stroke amplitudes by using the computational fluid dynamics (CFD).

METHOD

Wing Geometry

The tobacco hawkmoth *Manduca sexta* with its relatively large size is known for its flying and hovering abilities, and its wing characteristics is used for the current study. The wing planform used by Usherwood et al. (2002) is imitated for creating the wing model to be analyzed in the current study. Usherwood et al. (2002) derived the wing planform from the female hawkmoth *Manduca sexta* (F1) wing, and they treated the fore- and hind wings as a single wing.

In comparison with the real hawkmoth *Manduca sexta* wing (see Figure 1a), the model wing geometry referred to herein as the **MS** wing is shown in Figure 1b. The wing thickness (t_w) is taken as 0.3 mm which is approximately 1.6% of the mean aerodynamic chord length.

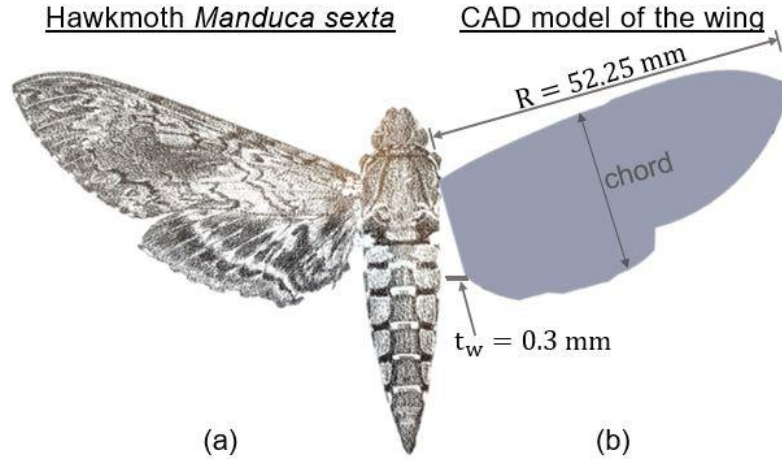


Figure 1: (a) Hawkmoth *Manduca sexta* [Brodsky, 1996] (b) CAD model of the MS wing similar to the study of Usherwood et al. (2002)

The morphological data about *Manduca sexta* wing [Bektas et al., 2018] in comparison with the current wing (MS) is given in Table 2 including single wing length (R), mean aerodynamic chord length (\bar{c}), single wing area (S) and dimensionless second moment of wing area (r_2/R).

Table 2: Morphological data of the hawkmoth *Manduca sexta* wing

Species	R [mm]	\bar{c} [mm]	S [mm ²]	r_2/R [-]	References
M1	48.50	18.37	891.00	0.514	[Willmott et al., 1997b]
F1	51.90	18.37	953.49	0.515	[Willmott et al., 1997b]
F2	52.10	18.88	983.48	0.518	[Willmott et al., 1997b]
Derived M1	48.30	18.30	887.00	0.520	[Liu et al., 1998]
Derived M1	48.30	18.30	883.89	-	[Nakata et al., 2012]
Derived M1	48.30	18.09	883.75	0.510	[Kim et al., 2014]
Derived F1	52.25	18.46	964.69	0.511	[Usherwood et al., 2002]
MS	52.25	18.46	964.60	0.511	Current study

Wing Kinematics

In the current study, the wing undergoing the harmonic motion in pure plunge is investigated. In order to do that, the wing geometry (MS) given in Figure 1b is placed with a fixed feathering angle ($\alpha=90^\circ$) along a specific stroke plane as shown in Figure 2. The simple sinusoidal motion is implemented to the wing model with a user-defined function (UDF). Eq. (1) and its time-derivative Eq. (2) are defined into the UDF code written in the C programming language to obtain the instantaneous flapping angles ($\phi(t)$) and to provide the plunge motion respectively:

$$\phi(t) = \Phi/2 \sin(2\pi ft) \quad (1)$$

$$d\phi(t)/dt = \Phi\pi f \cos(2\pi ft) \quad (2)$$

where Φ is the stroke amplitude, f is the wingbeat frequency, and t is the time.

The coordinate system used in the current study is given in Figure 2. The horizontal force (F_H) and vertical force (F_V) are along the X_G and Y_G directions, and the wing performs the pure plunge motion with respect to the Z_G -axis (see Figure 2a). The lift (L) and drag (D) directions are separately represented during both downstroke (see Figure 2b) and upstroke (see Figure 2c). When the wing is moving from up to down, the drag force is generated upward which is opposite to the direction of the motion as shown in Figure 2b.

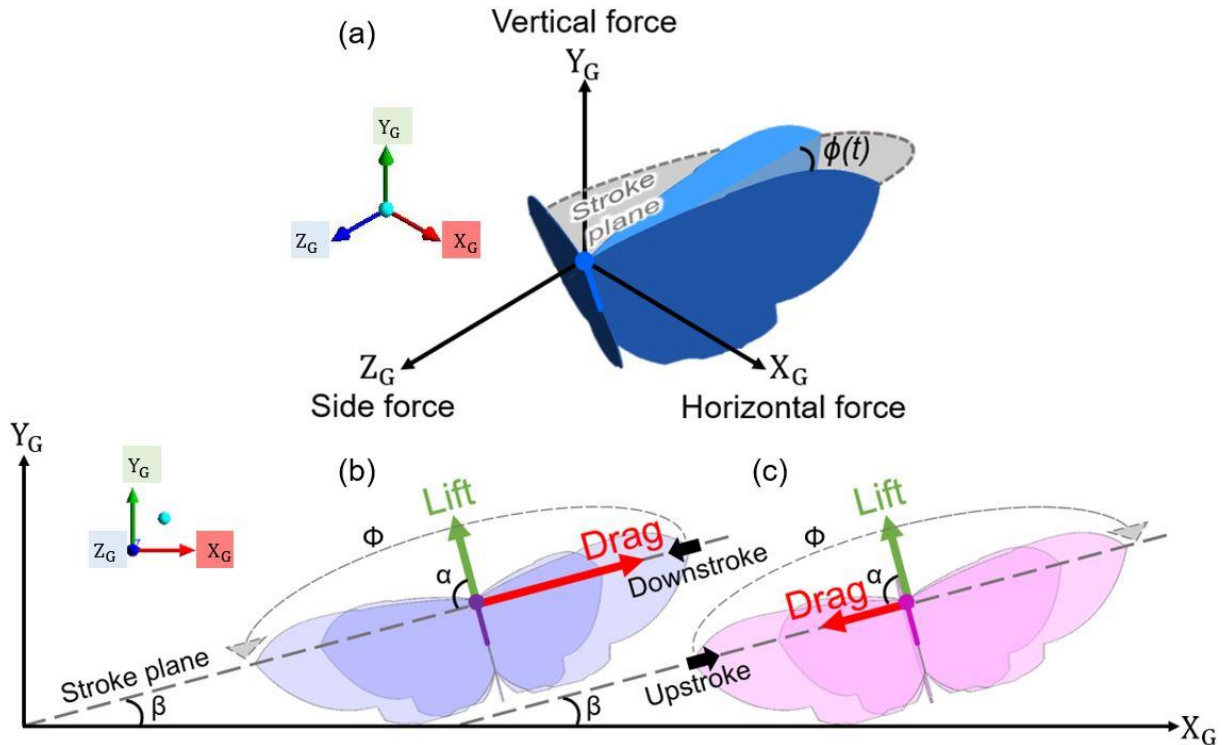


Figure 2: Coordinate definitions for (a) Horizontal force, vertical force and side force
(b) Lift and drag during the downstroke (c) Lift and drag during the upstroke

In this study, the CFD analyses are carried out where the fluid is chosen as air. Considering the air properties (density (ρ) is 1.225 kg/m^3 , and dynamic viscosity (μ) is $1.7894 \times 10^{-5} \text{ kg/m-s}$), the Reynolds number (Re) in hover mode is found by using Eq. (3):

$$Re = \frac{\rho U_{ref} \bar{c}}{\mu} \quad (3)$$

where a reference velocity (U_{ref}) is used because of not existing any freestream velocity. This reference velocity (U_{ref}) stands for the mean translational velocity at the radius of the second moment of wing area (r_2), and it is computed by using Eq. (4).

$$U_{ref} = 2f\Phi r_2 \quad (4)$$

By taking reference from the kinematic properties of the hawkmoth *Manduca sexta* wing given in Table 1, the MS wing flight parameters to be analyzed in hover mode are selected as shown in Table 3 including Reynolds number (Re), reference velocity (U_{ref}), wingbeat frequency (f), stroke plane angle (β) and stroke amplitude (Φ).

Table 3: Kinematic parameters to be used in the CFD analyses of the MS wing

Cases	Re [-]	U_{ref} [m/s]	f [s^{-1}]	β [$^\circ$]	Φ [$^\circ$]
1	3753	2.97	26.30	15	121.4
2	3728	2.95	26.10	15	121.4
3	4208	3.33	29.46	15	121.4
4	3842	3.04	29.46	15	110.8
5	3753	2.97	26.30	30	121.4
6	3753	2.97	26.30	90	121.4

In Table 3, kinematic parameters for Case 1 are taken from the properties of F1-Mean wing kinematics indicated in Table 1. By decreasing and increasing the wingbeat frequency respectively, Case 2 and Case 3 vary from Case 1. For Case 4, the stroke amplitude is decreased while the other conditions are the same as in Case 3. Additionally, Cases 1, 5 and 6 are investigated to observe the effects of the stroke plane angle.

Computational Method and Governing Equations

In the current study, the unsteady flapping motion is divided into 4 regions as half-upstroke, half-downstroke and second half of both downstroke and upstroke, respectively. A computational method, namely computational fluid dynamics (CFD) is used to obtain the instantaneous aerodynamic forces of the MS wing in the cases given in Table 3. Moreover, it can be simulated that the flow-fields around the MS wing by using the CFD. In order to perform all following CFD simulations, ANSYS/Fluent is used at 2 CPU 16 core Intel Xeon Z640 workstation computer. For all analyses, an O-type computational domain is placed with a radius of 1 m, and the boundary conditions are set as pressure-outlet for the freestream and as wall for the wing as indicated in Figure 3a. In addition, Figure 3b shows the boundary layers with the first layer thickness of $0.002c$ and finer mesh close to the MS wing. All of the grids are also created by using ANSYS/Meshing in this study.

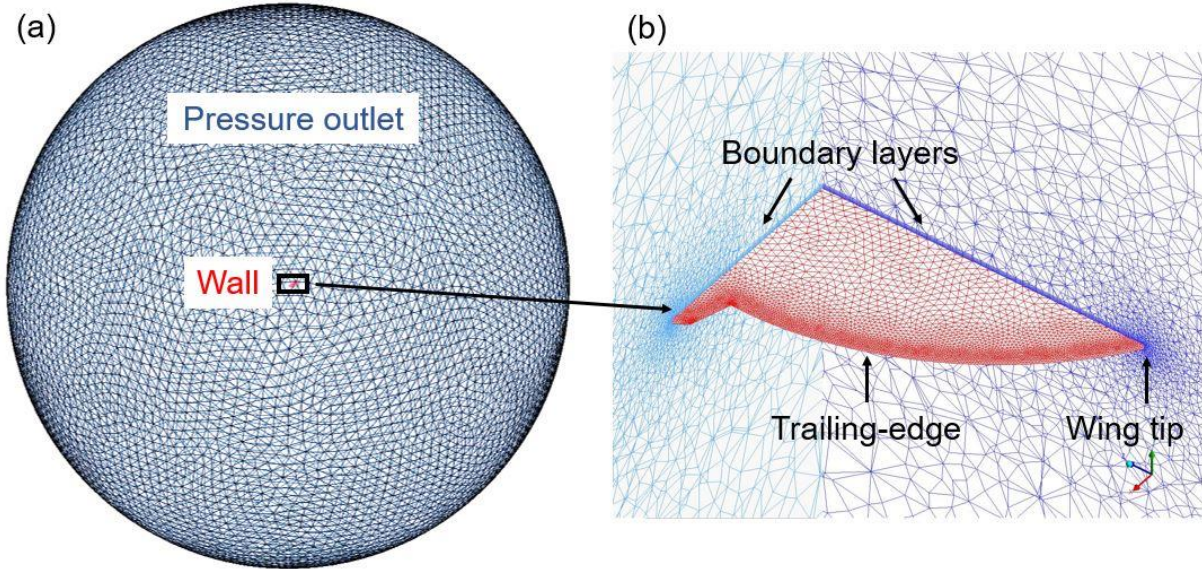


Figure 3: (a) Boundary conditions for the fluid analysis (pressure outlet = blue; wall = red)
(b) Closer view to the unstructured mesh and boundary layers around the wing

In hover mode, moving all grids by using the dynamic mesh is suitable for the unstructured grids with tetrahedral elements shown in Figure 3. The simple sinusoidal motion is applied by adding the compiled UDF into the dynamic mesh option in ANSYS/Fluent. The smoothing option in dynamic mesh is used for repositioning interior nodes to lower the maximum skewness of the mesh while the wing is plunging up and down. SIMPLE scheme is used for pressure-velocity coupling, and Least Squares Cell Based method is chosen. Since the three-dimensional bio-inspired MS wing model is aerodynamically operated at low-Reynolds-numbers (see Table 3, $Re < 10^4$), the flow is chosen as a laminar flow model. For three-dimensional, unsteady and incompressible flow conditions, the governing Navier-Stokes equations are given in Eqs. (5)-(8):

$$\frac{\partial u}{\partial x} + \frac{\partial v}{\partial y} + \frac{\partial w}{\partial z} = 0 \quad (5)$$

$$\rho \left(\frac{\partial u}{\partial t} + u \frac{\partial u}{\partial x} + v \frac{\partial u}{\partial y} + w \frac{\partial u}{\partial z} \right) = -\frac{\partial p}{\partial x} + \mu \left(\frac{\partial^2 u}{\partial x^2} + \frac{\partial^2 u}{\partial y^2} + \frac{\partial^2 u}{\partial z^2} \right) \quad (6)$$

$$\rho \left(\frac{\partial v}{\partial t} + u \frac{\partial v}{\partial x} + v \frac{\partial v}{\partial y} + w \frac{\partial v}{\partial z} \right) = -\frac{\partial p}{\partial y} + \mu \left(\frac{\partial^2 v}{\partial x^2} + \frac{\partial^2 v}{\partial y^2} + \frac{\partial^2 v}{\partial z^2} \right) \quad (7)$$

$$\rho \left(\frac{\partial w}{\partial t} + u \frac{\partial w}{\partial x} + v \frac{\partial w}{\partial y} + w \frac{\partial w}{\partial z} \right) = -\frac{\partial p}{\partial z} + \mu \left(\frac{\partial^2 w}{\partial x^2} + \frac{\partial^2 w}{\partial y^2} + \frac{\partial^2 w}{\partial z^2} \right) \quad (8)$$

where u , v , w are the velocity components in x , y , z directions; p is the pressure. The dimensionless aerodynamic force coefficients (C_F) are found from Eq. (9):

$$C_F = \frac{F}{\frac{1}{2} \rho U_{ref}^2 S} \quad (9)$$

where F demonstrates the aerodynamic forces such as vertical force, horizontal force and side force.

Mesh Refinement Study

A mesh refinement study is performed for Case 6 which uses the MS wing hovering along a vertical stroke plane ($\beta = 90^\circ$). The unstructured volume grids with different element numbers are analyzed at the time step of 0.0001s. The element numbers for each mesh domain with corresponding the time required to complete the one period of the numerical analysis are given in Table 4. Figure 4 shows the instantaneous stroke angle and instantaneous aerodynamic force coefficients in the $[1T \ 2T]$ interval where T represents the period.

Table 4: Mesh refinement study

Mesh type	Number of elements	Time step increment (Δt)	Analysis time per period
Coarse	1393423	0.0001 s	15 h 30 m
Medium	2020648	0.0001 s	26 h 10 m
Fine	7226635	0.0001 s	109 h 20 m

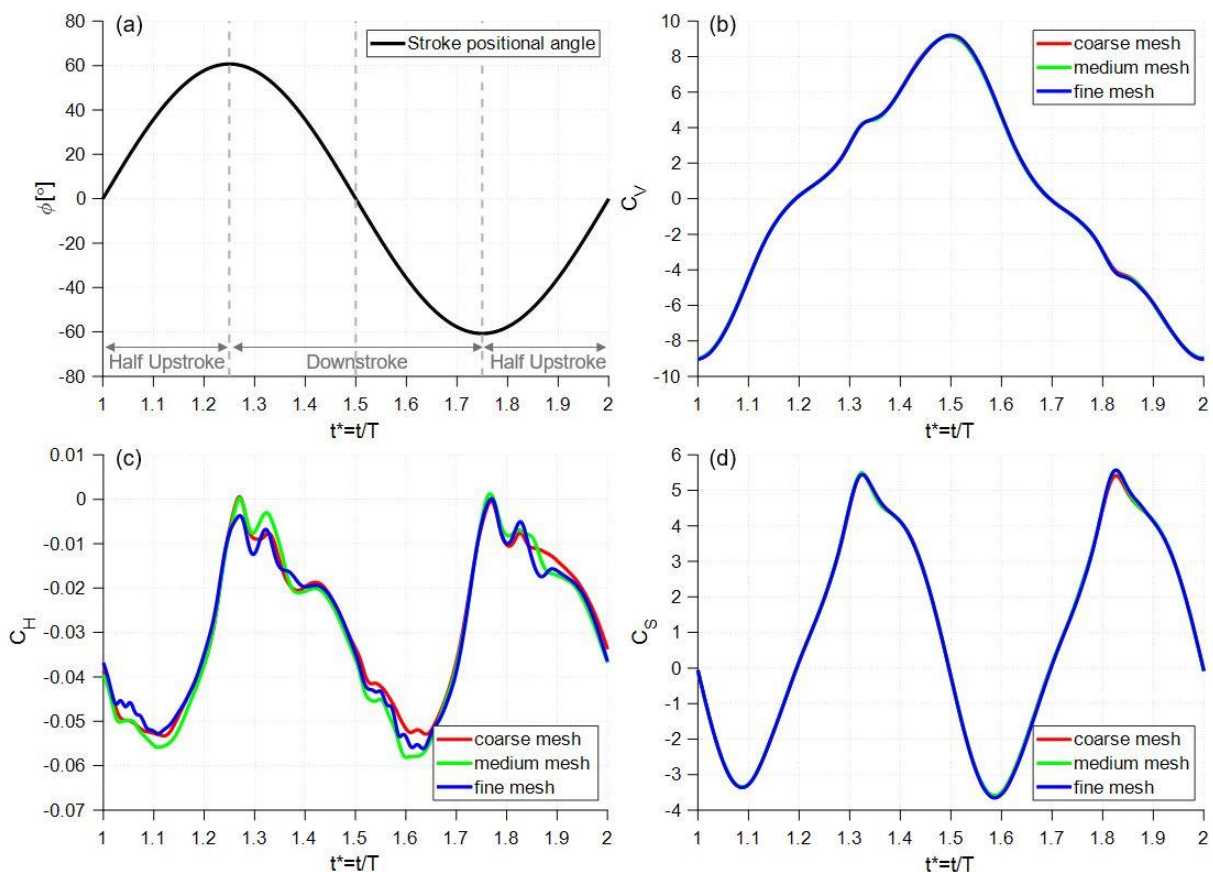


Figure 4: Mesh refinement study (a) Instantaneous stroke angle (b) Vertical force coefficient (c) Horizontal force coefficient (d) Side force coefficient

In the mesh refinement study, the analyses with the coarse, medium and fine meshes give the same results for the vertical force coefficients (see Figure 4b) and for the side force coefficients (see Figure 4d). The time required to complete the fine mesh analysis is too much (see Table 4), consequently the medium mesh with closer aerodynamic force coefficients to the fine mesh (see Figure 4) is selected for the following analyses.

Time Step Size Refinement Study

A refinement study for the time is also carried out for Case 6 with medium mesh type. The CFD simulations are carried out with three different time step sizes as given in Table 5. All simulations are run for 20 sub-iterations per time step. Figure 5 represents the instantaneous stroke angle starting with the half-upstroke and instantaneous aerodynamic force coefficients in the $[1T \ 2T]$ interval where T is the period ($T=1/f$).

Table 5: Time step size refinement study

Mesh type	Time step increment	Iteration per period ($T/\Delta t$)	Analysis time per period
Medium	0.00020 s	190	16 h 25 m
Medium	0.00010 s	380	26 h 10 m
Medium	0.00005 s	760	36 h 15 m

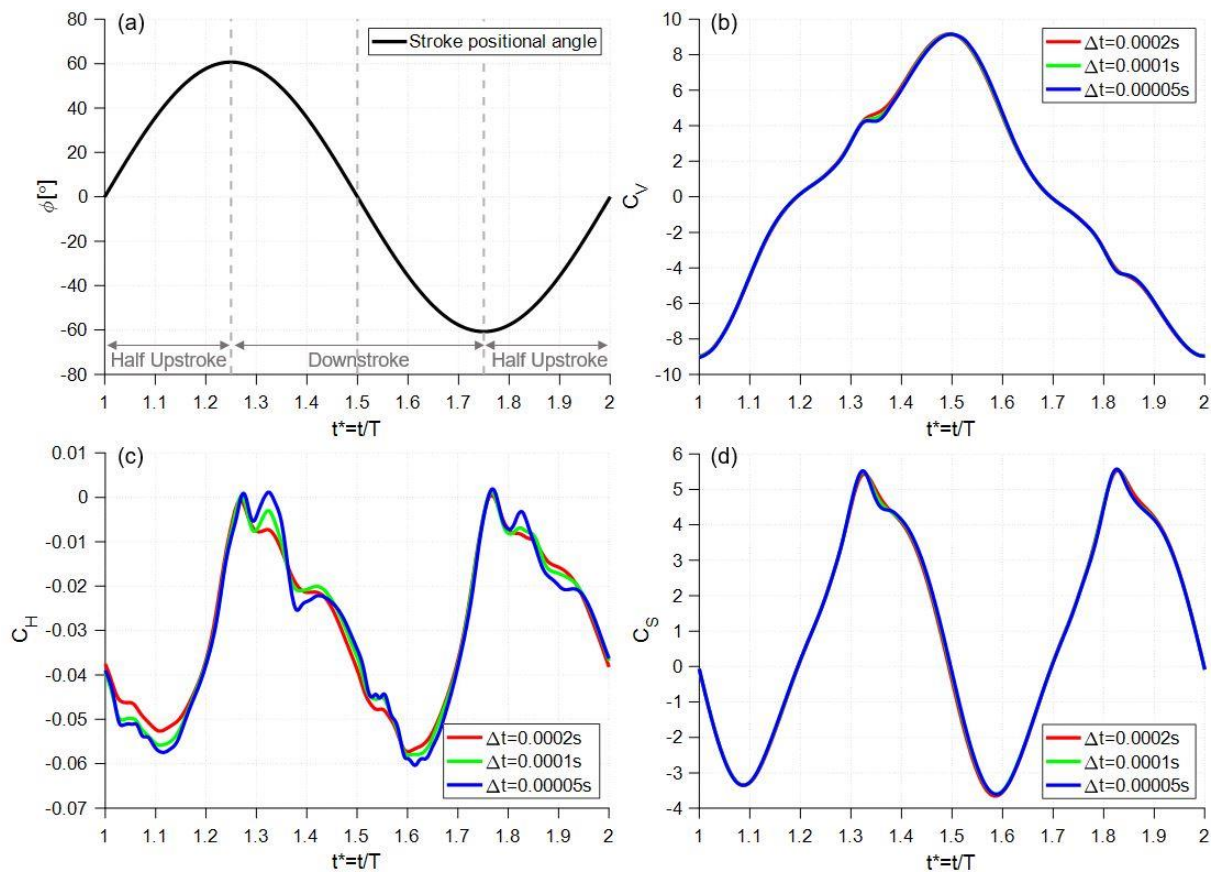


Figure 5: Time step size refinement study (a) Instantaneous stroke angle (b) Vertical force coefficient (c) Horizontal force coefficient (d) Side force coefficient

As it can be seen from Figure 5, a time step of 0.0002s for the plunging motion has some differences compared to the finer cases close to the peaks. Therefore, 380 iteration per period with the time step of 0.0001s is selected to analyze all the cases shown in Table 3.

The similarity of the results of both grid and time refinement studies are important to validate the numerical analyses. When the accuracy and time required to complete the one period of the analyses are considered, the following CFD analyses are performed for the medium mesh with the time step of 0.0001s.

RESULTS

Aerodynamic Force Comparison for Case 1, Case 2, Case 3 and Case 4

In Figure 6, the unsteady aerodynamic forces are obtained for Cases 1, 2, 3 and 4 given in Table 3. In order to observe the quasi-steady solutions, all results are presented in the $[4T \ 5T]$ interval by neglecting the initial impulsive start. The wing position for each quarter stroke during one period is also represented in Figure 6. Figure 6 shows the instantaneous stroke positional angle and instantaneous aerodynamic forces during one cycle starting with the half-upstroke.

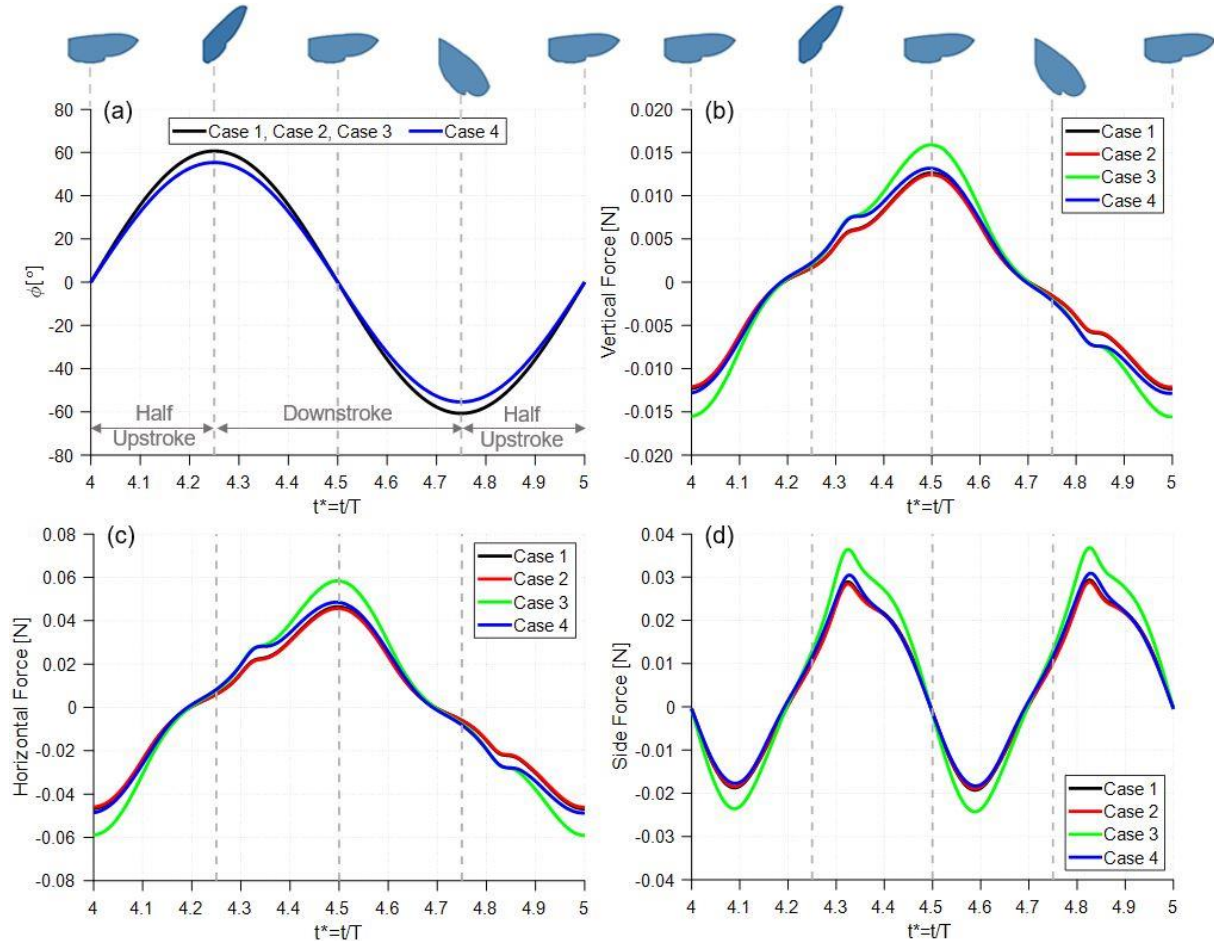


Figure 6: The results for Cases 1, 2, 3 and 4 (a) Instantaneous stroke angle (b) Vertical force (c) Horizontal force (d) Side force

For all cases investigated here, the maximum values of both vertical forces (see Figure 6b) and horizontal forces (see Figure 6c) are obtained at the half-downstroke corresponding to $t^*=4.5$. However, the side forces having two peaks (see Figure 6d) are maximum at $t^*=4.32$ and $t^*=4.82$. The aerodynamic force maximum amplitudes are found to be the biggest in Case 3 (plotted with green lines) which has the highest values of both wingbeat frequency and stroke amplitude and consequently the maximum reference velocity. In addition, they are the smallest in Case 2 (plotted with red lines) which has the lowest wingbeat frequency and the minimum reference velocity.

Aerodynamic Force Comparison for Case 1, Case 5 and Case 6

Cases 1, 5 and 6 are numerically analyzed to see the effects of stroke plane angle under the same stroke amplitude and same wingbeat frequency and consequently the same stroke positional angle (see Figure 7a). Figure 7 shows the graphs of unsteady aerodynamic forces with the wing positions at each quarter stroke during the $[4T \ 5T]$ interval.

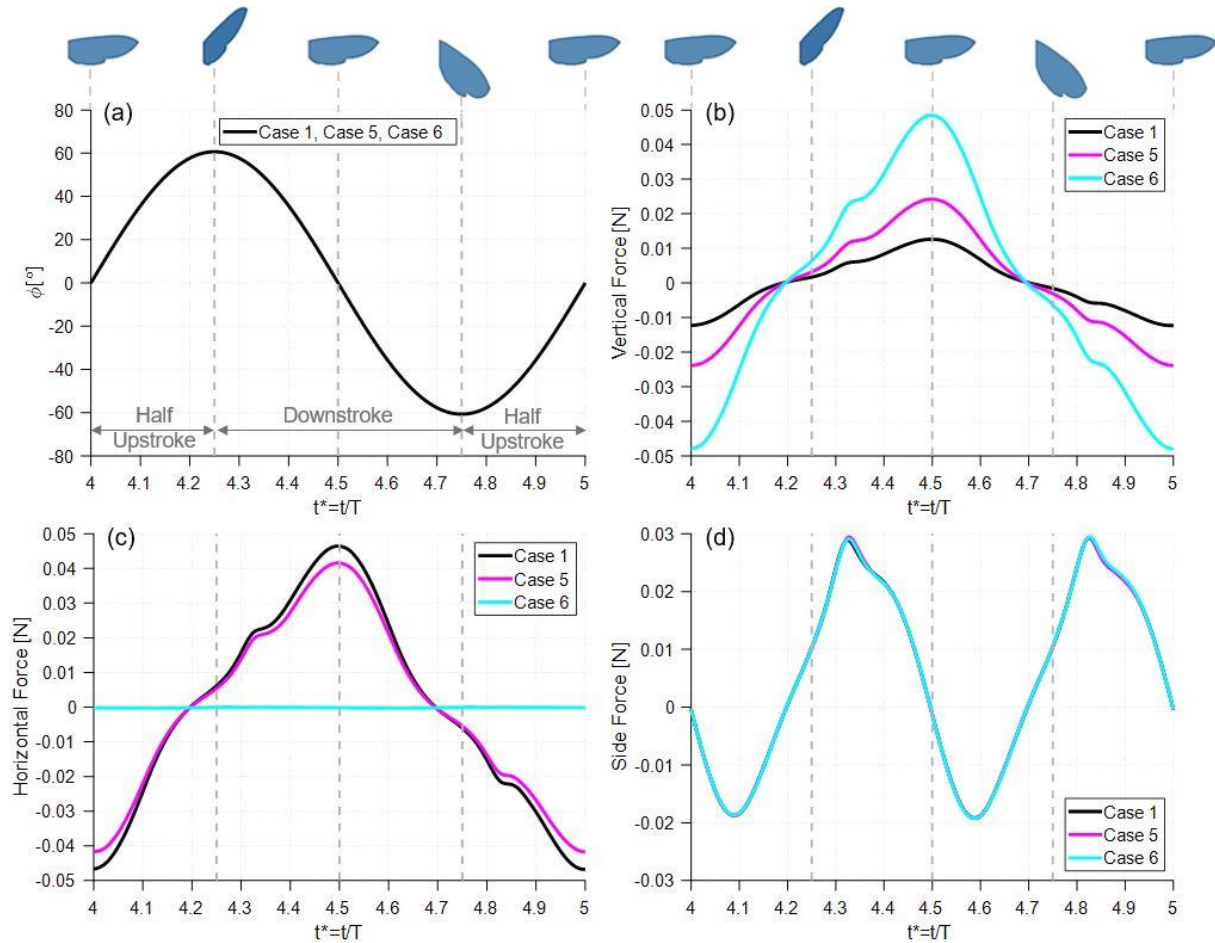


Figure 7: The results for Cases 1, 5 and 6 (a) Instantaneous stroke angle (b) Vertical force (c) Horizontal force (d) Side force

The vertical force maximum amplitude (see Figure 7b) is found to be the biggest for Case 6 (plotted with cyan lines) where the wing hovers along the vertical stroke plane ($\beta = 90^\circ$), and it decreases when the stroke plane angle decreases to 15° . Unlike the vertical force, the horizontal force maximum amplitude (see Figure 7c) is the smallest for Case 6, and it increases when the stroke plane angle decreases to 15° . Additionally, it can be noted that changing only the stroke plane angle is not much affecting to the side forces (see Figure 7d).

In the current study, the CFD analyses are performed for the single MS wing. Considering the two wings, the mean aerodynamic forces are calculated as twice of the CFD results obtained for all cases analyzed in hover mode. For two MS wings, the mean vertical force ($\overline{F_V}$) and the mean horizontal force ($\overline{F_H}$) together with their mean resultant forces ($\overline{F_R}$) are demonstrated in Table 6.

Table 6: The mean aerodynamic forces for two MS wings

Cases	$\overline{F_V}$ [mN]	$\overline{F_H}$ [mN]	$\overline{F_R}$ [mN]
1- $U_{ref} = 2.97\text{m/s}$; $f = 26.30\text{s}^{-1}$; $\beta = 15^\circ$; $\Phi = 121.4^\circ$	0.270310	-0.17278	0.320812
2- $U_{ref} = 2.95\text{m/s}$; $f = 26.10\text{s}^{-1}$; $\beta = 15^\circ$; $\Phi = 121.4^\circ$	0.257670	-0.19012	0.320218
3- $U_{ref} = 3.33\text{m/s}$; $f = 29.46\text{s}^{-1}$; $\beta = 15^\circ$; $\Phi = 121.4^\circ$	0.346182	-0.17578	0.388253
4- $U_{ref} = 3.04\text{m/s}$; $f = 29.46\text{s}^{-1}$; $\beta = 15^\circ$; $\Phi = 110.8^\circ$	0.306416	-0.10936	0.325347
5- $U_{ref} = 2.97\text{m/s}$; $f = 26.30\text{s}^{-1}$; $\beta = 30^\circ$; $\Phi = 121.4^\circ$	0.231676	-0.21282	0.314589
6- $U_{ref} = 2.97\text{m/s}$; $f = 26.30\text{s}^{-1}$; $\beta = 90^\circ$; $\Phi = 121.4^\circ$	-0.02898	-0.29738	0.298789

As it can be seen from Table 6, the mean vertical force decreases with the decreasing wingbeat frequency (see Cases 1&2), and it increases with the increasing wingbeat frequency (see

Cases 1&3). For the cases having the same wingbeat frequency and same stroke plane angle, the mean vertical force decreases while the stroke amplitude decreases (see Cases 3&4). The case with a higher stroke plane angle generates a lower mean vertical force (see Cases 1, 5&6). When all of these factors are taken into account, the mean vertical force has the maximum value in Case 3 where \bar{F}_V is approximately 0.35 mN. However, the force required to balance the insect mass is approximately 15 mN which is forty times of our maximum \bar{F}_V calculated from the CFD analyses. For this reason, these simplified cases are actually not enough to hover of *Manduca Sexta* because of the symmetrical plunging motion of the rigid and flat wing model. These are just to see the effects of the kinematic parameters and to observe the lift capacities of the MS wing.

Flow-field during the Downstroke for Case 1

The flow-field occurred around the MS wing in Case 1 is shown in Figure 8 during the downstroke. The static pressure contours are drawn where the atmospheric pressure (P_∞) is 101325 Pa. For the static gauge pressure distributions on the lower and upper surfaces of the MS wing (see Figure 8a), the red color demonstrates the high-pressure region ($P-P_\infty=20$ Pa) while the blue color demonstrates the low-pressure region ($P-P_\infty=-20$ Pa). The iso-vorticity values are found from the ratio between the reference velocity and the mean aerodynamic chord length. For the iso-surface of Z-vorticity distributions (see Figure 8b), the red regions indicate the positive iso-vorticity (counter-clockwise) while the blue regions indicate the negative iso-vorticity (clockwise).

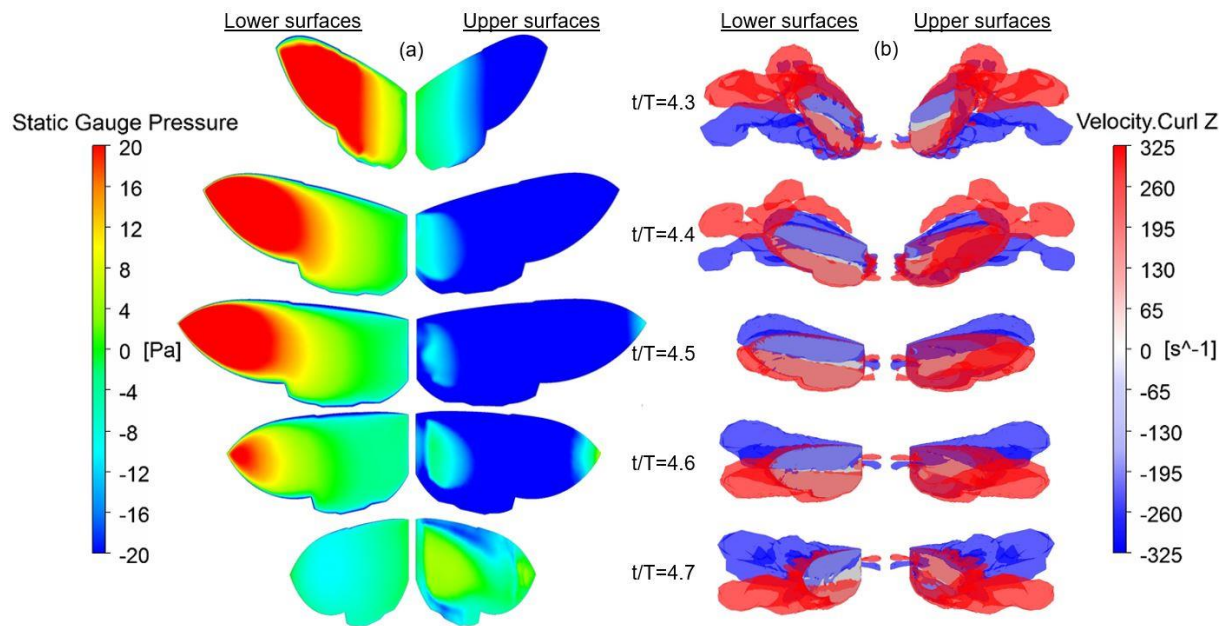


Figure 8: The results for Case 1 during the downstroke (a) Static pressure distributions (b) Iso-surfaces of Z-vorticity distributions

The higher-pressure regions (see Figure 8a) and the stronger vortices (see Figure 8b) are clearly seen at the wing tips. At the beginning of the downstroke ($t/T=4.3$), the highest pressure is obtained on the lower surface; and more complex iso-vorticity is seen because of the effects of the previous upstroke motion. During the downstroke, the pressure on the lower surface is started to decrease. Meanwhile, a suction region is occurred ($P-P_\infty=-20$ Pa) on the upper surfaces of the wing. Additionally, the positive iso-vorticity is placed around the trailing edge, and the negative iso-vorticity is placed around the leading edge during the downstroke.

Two-dimensional distributions for both static gauge pressure and iso-surface of Z-vorticity are represented in Figure 9 to clearly see the results for chordwise. The contours at the half-downstroke ($t/T=4.5$) are drawn at three different span locations from the wing root namely $R/4$, $R/2$ and $3R/4$ positions where R denotes the single wing length.

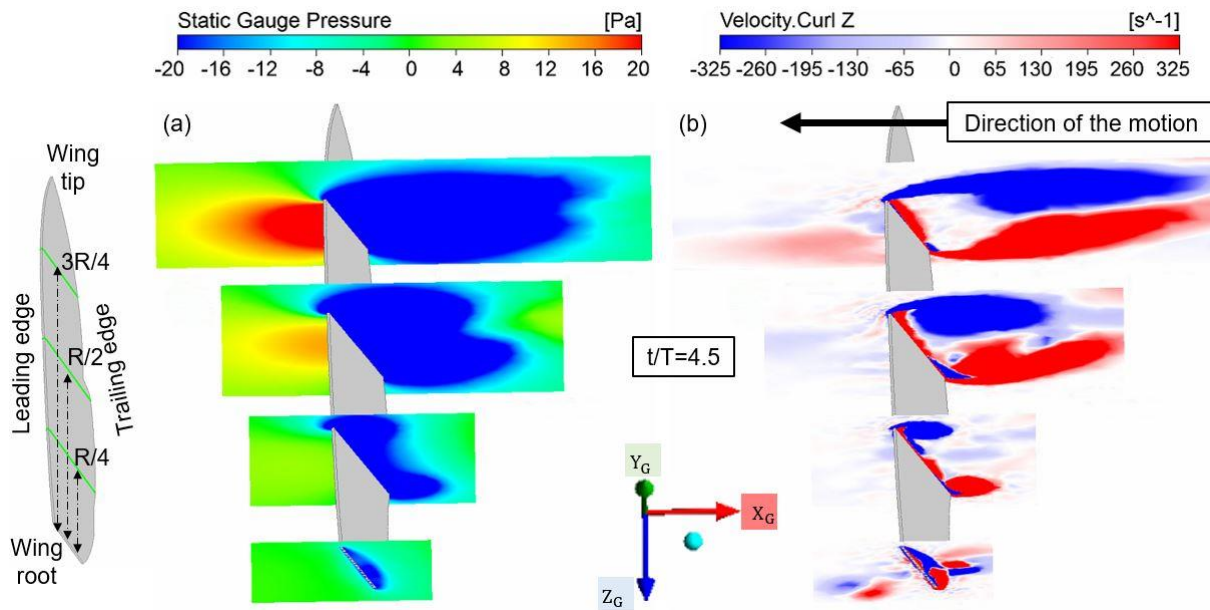


Figure 9: Closer view to the results of Case 1 at the half downstroke where $t/T=4.5$
 (a) Static pressure contours around the MS wing (b) Iso-surfaces of Z-vorticity contours around the MS wing

As it can be understood from Figure 9 where the planes are set from the wing root with quarter ranges, the high pressure and high vorticity are clearly observed at the wing tip. At the half-downstroke ($t^*=4.5$), a suction region is occurred on the upper surface of the wing (see Figure 9a), and this is where the high iso-surface of Z-vorticity is obtained (see Figure 9b). While the maximum pressure is seen on the lower wing surface, the majority of vorticity is generated on the upper surface of the wing. The formation of the leading edge vortex and its grow from the root towards the tip are clearly visualized in Figure 9b. Moreover, the iso-surface of Z-vorticity direction is obviously seen in the opposite direction of the motion. There is also a counter-clockwise (red color) trailing edge vortex which is very dominant at the wing tip.

CONCLUSION

This paper is a basis for the investigation of the unsteady aerodynamics of a flapping wing model mimicked from the hawkmoth *Manduca sexta*. The MS wing model hovering along the inclined and vertical stroke planes is investigated under the pure plunge motion. A single degree-of-freedom motion with the time varying stroke positional angle is provided by defining a sinusoidal motion into the user defined function (UDF). Computational fluid dynamics (CFD) is used to obtain the aerodynamic forces and to simulate both the static pressure distributions and the iso-surface of Z-vorticity distributions. In the current study, different kinematic parameters namely wingbeat frequency, stroke plane angle and stroke amplitude are considered with respect to their effects on the aerodynamic forces. For the MS wing model analyzed in hover mode with the pure plunge motion, the parameters which increase the mean vertical force are observed for the high wingbeat frequency, high stroke amplitude and consequently high reference velocity. In addition, it is seen that the mean vertical force decreases when the stroke plane angle increases. Moreover, a negative mean vertical force is found when the vertical stroke plane is used. The mean horizontal forces are obtained as negative for all cases investigated. Therefore, the thrust is generated in the current study. Finally, the maximum vertical forces are obtained at the half-downstroke ($t/T=4.5$) where the high-pressure region is occurred on the lower wing surface and the high iso-surface of Z-vorticity is seen on the upper wing surface. The studies will be continued with aeroelastic analyses by adding the vein structures into the MS wing and by improving the wing motion.

ACKNOWLEDGEMENT

This work is supported by TÜBİTAK Project No: 116M273.

References

- Ames, R.G. (2001) *On the Flowfield and Forces Generated by a Rectangular Wing Undergoing Moderate Reduced Frequency Flapping at Low Reynolds Number*, PhD Dissertation, Department of Aerospace Engineering, Georgia Institute of Technology, April 2001.
- Bektas, M., Kurtulus, D.F. and Guler, M.A. (2018) *Steady-State CFD Analysis of 3D Bio-inspired Flapping Wing Models*, International Symposium on Sustainable Aviation, Rome, Italy, 9-11 July 2018.
- Brodsky, A.K. (1996) *The Evolution of Insect Flight*, Oxford: Oxford University Press, 1996.
- Combes, S.A. and Daniel, T.L. (2003) *Flexural Stiffness in Insect Wings. I. Scaling and the Influence of Wing Venation*, Journal of Experimental Biology, Vol. 206, p: 2979-2987, June 2003.
- Kim, J.K. and Han, J.H. (2014) *A Multibody Approach for 6-DOF Flight Dynamics and Stability Analysis of the Hawkmoth Manduca Sexta*, Bioinspiration & Biomimetics, Vol. 9, No. 1, January 2014.
- Kurtulus, D.F. (2011a) *Introduction to Micro Air Vehicles: Concepts, Design and Applications*, Recent Developments in Unmanned Aircraft Systems (UAS, including UAV and MAV), Von Karman Institute for Fluid Dynamics, p: 187-217, April 2011.
- Kurtulus, D.F. (2011b) *Unsteady Aerodynamics of Flapping Aerofoils: Case Studies with Experimental, Numerical, Theoretical and Soft Computing Methods*, Recent Developments in Unmanned Aircraft Systems (UAS, including UAV and MAV), Von Karman Institute for Fluid Dynamics, p: 219-255, April 2011.
- Kurtulus, D.F. (2017) *MHA Tasarımlarına İlham Veren Kanatlı Böceklerin Uçuş Özellikleri*, Sustainable Aviation Research Society, Vol. 2, No. 2, p: 66-75, December 2017.
- Kurtulus, D.F. (2018) *Aerodynamic Loads of Small-Amplitude Pitching NACA 0012 Airfoil at Reynolds Number of 1000*, AIAA Journal, Vol. 56, No. 8, p: 3328-3331, August 2018.
- Kurtulus, D.F., David, L., Farcy, A. and Alemdaroglu, N. (2006a) *A Parametrical Study with Laser Sheet Visualization for an Unsteady Flapping Motion*, 36th AIAA Fluid Dynamics Conference and Exhibit, San Francisco, California, 5-8 June 2006.
- Kurtulus, D.F., David, L., Farcy, A. and Alemdaroglu, N. (2006b) *Laser Sheet Visualization for Flapping Motion in Hover*, 44th AIAA Aerospace Sciences Meeting and Exhibit, Reno, Nevada, 9-12 January 2006.
- Kurtulus, D.F., David, L., Farcy, A. and Alemdaroglu, N. (2008) *Aerodynamic Characteristics of Flapping Motion in Hover*, Experiments in Fluids, Vol. 44, No. 1, p: 23-36, January 2008.

- Kurtulus, D.F., Farcy, A. and Alemdaroglu, N. (2004) *Numerical Calculation and Analytical Modelization of Flapping Motion in Hover*, Proceeding of 1st European Micro Air Vehicle Conference and Flight Competition, Braunschweig, Germany, 13-14 July 2004.
- Kurtulus, D.F., Farcy, A. and Alemdaroglu, N. (2005) *Unsteady Aerodynamics of Flapping Airfoil in Hovering Flight at Low Reynolds Numbers*, 43rd AIAA Aerospace Sciences Meeting and Exhibit, Reno, Nevada, 10-13 January 2005.
- Liu, H. and Kawachi, K. (1998) *A Numerical Study of Insect Flight*, Journal of Computational Physics, Vol. 146, p: 124-156, October 1998.
- Maxworthy, T. (1981) *The Fluid Dynamics of Insect Flight*, Annual Review of Fluid Mechanics, Vol. 13, p: 329-350, January 1981.
- Nakata, T. and Liu, H. (2012) *Aerodynamic Performance of a Hovering Hawkmoth with Flexible Wings: A Computational Approach*, Proceedings of the Royal Society B, Vol. 279, No. 1729, p: 722-731, February 2012.
- Shyy, W., Lian, Y., Tang, J., Liu, H., Trizila, P., Stanford, B., Bernal, L., Cesnik, C., Friedmann, P. and Ifju, P. (2008) *Computational Aerodynamics of Low Reynolds Number Plunging, Pitching and Flexible Wings for MAV Applications*, 46th AIAA Aerospace Sciences Meeting and Exhibit, Reno, Nevada, 7-10 January 2008.
- Usherwood, J.R. and Ellington, C.P. (2002) *The Aerodynamics of Revolving Wings. I. Model Hawkmoth Wings*, Journal of Experimental Biology, Vol. 205, p: 1547-1564, March 2002.
- Willmott, A.P. and Ellington, C.P. (1997a) *The Mechanics of Flight in the Hawkmoth Manduca Sexta. I. Kinematics of Hovering and Forward Flight*, Journal of Experimental Biology, Vol. 200, p: 2705-2722, August 1997.
- Willmott, A.P. and Ellington, C.P. (1997b) *The Mechanics of Flight in the Hawkmoth Manduca Sexta. II. Aerodynamic Consequences of Kinematic and Morphological Variation*, Journal of Experimental Biology, Vol. 200, p: 2723-2745, August 1997.